Atmos. Chem. Phys., 16, 15593–15604, 2016
www.atmos-chem-phys.net/16/15593/2016/
doi:10.5194/acp-16-15593-2016

Atmospheric Chemistry and Physics
Open Access
EGU

Nighttime atmospheric chemistry of iodine

Alfonso Saiz-Lopez[1], John M. C. Plane[2], Carlos A. Cuevas[1], Anoop S. Mahajan[3], Jean-François Lamarque[4], and Douglas E. Kinnison[4]

[1]Department of Atmospheric Chemistry and Climate, Institute of Physical Chemistry Rocasolano, CSIC, Madrid, Spain
[2]School of Chemistry, University of Leeds, Leeds, UK
[3]Indian Institute of Tropical Meteorology, Pune, India
[4]Atmospheric Chemistry Observations & Modeling Laboratory, National Center for Atmospheric Research, Boulder, 10 Colorado, USA

Correspondence to: Alfonso Saiz-Lopez (a.saiz@csic.es)

Received: 18 May 2016 – Published in Atmos. Chem. Phys. Discuss.: 15 June 2016
Revised: 2 December 2016 – Accepted: 5 December 2016 – Published: 19 December 2016

Abstract. Little attention has so far been paid to the nighttime atmospheric chemistry of iodine species. Current atmospheric models predict a buildup of HOI and I_2 during the night that leads to a spike of IO at sunrise, which is not observed by measurements. In this work, electronic structure calculations are used to survey possible reactions that HOI and I_2 could undergo at night in the lower troposphere, and hence reduce their nighttime accumulation. The new reaction $NO_3 + HOI \rightarrow IO + HNO_3$ is proposed, with a rate coefficient calculated from statistical rate theory over the temperature range 260–300 K and at a pressure of 1000 hPa to be $k(T) = 2.7 \times 10^{-12}\ (300\,\mathrm{K}/T)^{2.66}\ \mathrm{cm^3\ molecule^{-1}\ s^{-1}}$. This reaction is included in two atmospheric models, along with the known reaction between I_2 and NO_3, to explore a new nocturnal iodine radical activation mechanism. The results show that this iodine scheme leads to a considerable reduction of nighttime HOI and I_2, which results in the enhancement of more than 25 % of nighttime ocean emissions of $HOI + I_2$ and the removal of the anomalous spike of IO at sunrise. We suggest that active nighttime iodine can also have a considerable, so far unrecognized, impact on the reduction of the NO_3 radical levels in the marine boundary layer (MBL) and hence upon the nocturnal oxidizing capacity of the marine atmosphere. The effect of this is exemplified by the indirect effect on dimethyl sulfide (DMS) oxidation.

1 Introduction

Active nighttime iodine chemistry was first evidenced a decade ago when it was shown that nocturnal I_2 emitted by macroalgae could react with NO_3 leading to the formation of IO and OIO, which were measured in the coastal marine boundary layer (MBL) at Mace Head, Ireland (Saiz-Lopez and Plane, 2004). The nitrate radical has also been recently suggested as a nocturnal loss of CH_2I_2, which helps to reconcile observed and modelled concentrations of this iodocarbon over the remote MBL (Carpenter et al., 2015). However, most of the work on reactive atmospheric iodine has focused on the use of daytime observations and models to assess its role in the catalytic destruction of ozone and the oxidizing capacity of the troposphere (e.g. Saiz-Lopez et al., 2012b, and references therein). In the MBL, iodine-catalysed along with bromine-catalysed ozone destruction contributes up to 45 % of the observed daytime depletion (Read et al., 2008; Mahajan et al., 2010a), although this contribution shows large geographical variability (Mahajan et al., 2012; Gómez Martín et al., 2013; Prados-Roman et al., 2015b; Volkamer et al., 2015). Iodine compounds have also been implicated in the formation of aerosols, although the mechanisms and magnitudes of these processes are not fully understood (Hoffmann et al., 2001; O'Dowd et al., 2002; McFiggans et al., 2004; Gómez Martín et al., 2013; Allan et al., 2015; Roscoe et al., 2015). Reactive forms of inorganic iodine may also contribute to the oxidation of elemental mercury over the tropical oceans (Wang et al., 2014). In recent years, iodine sources and chemistry have also been implemented in global models

demonstrating the effect of iodine chemistry in the oxidation capacity of the global marine troposphere (Ordóñez et al., 2012; Saiz-Lopez et al., 2012a, 2014; Sherwen et al., 2016).

Iodine is emitted into the atmosphere from the ocean surface in both organic and inorganic forms. The main organic compounds emitted are methyl iodide (CH_3I), ethyl iodide (C_2H_5I), propyl iodide (1- and 2-C_3H_7I), chloroiodomethane (CH_2ICl), bromoiodomethane (CH_2IBr) and diiodomethane (CH_2I_2) (Carpenter, 2003; Butler et al., 2007; Jones et al., 2010; Mahajan et al., 2012). However, these organic compounds contribute only up to a fourth of the MBL iodine loading (Jones et al., 2010; Mahajan et al., 2010a; Großmann et al., 2013; Prados-Roman et al., 2015b). Inorganic emissions of HOI and I_2, which result from the deposition of O_3 at the ocean surface and subsequent reaction with I^- ions in the surface microlayer, account for the main source of iodine in the MBL (Carpenter et al., 2013). Recent laboratory experiments have shown that HOI is the major compound emitted and provided parameterizations of the fluxes of both species depending on wind speed, temperature, and the concentrations of O_3 and I^- (Carpenter et al., 2013; MacDonald et al., 2014). These parameterized fluxes of HOI and I_2 have then been used in a one-dimensional model to study the diurnal evolution of the IO and I_2 mixing ratios at the Cape Verde Atmospheric Observatory (CVAO) (Carpenter et al., 2013; Lawler et al., 2014). The model simulations replicate well the levels and general diurnal profiles of IO and I_2, although an early morning "dawn spike" in IO is predicted by the models but has not been observed (Read et al., 2008; Mahajan et al., 2010a). The morning peak predicted by current iodine chemistry models is due to a buildup of the emitted I_2 and HOI (which is converted into IBr / ICl through heterogeneous sea-salt recycling) over the course of the night, followed by rapid photolysis at sunrise.

Traditionally it has been thought that iodine chemistry has a negligible effect on oxidizing capacity of the nocturnal marine atmosphere. As a consequence, unlike the demonstrated effect of iodine on the levels of daytime oxidants, the impact of active iodine upon the main nighttime oxidant, NO_3, remains an open question. This is important given that in many parts of the ocean the NO_3 + dimethyl sulfide (DMS) reaction is at least as important as OH + DMS in oxidizing DMS (Allan et al., 2000), and hence a reduction of NO_3 may have an effect in the production of SO_2 and methane sulfonic acid (MSA). Here, we discuss possible mechanisms of nighttime iodine radical activation and their potential effect on nighttime iodine ocean fluxes and the currently modelled dawn spike in IO. A new reaction of HOI with NO_3 is proposed, supported by theoretical calculations. We explore the implications of this new reaction both for iodine and NO_3 chemistries.

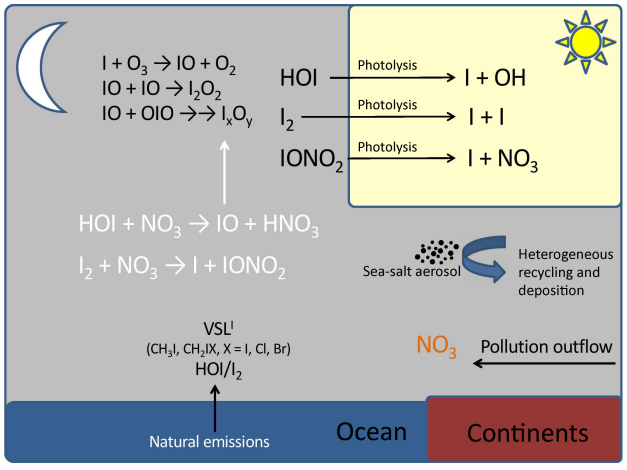

Figure 1. New nocturnal iodine chemistry (in white) implemented in the THAMO and CAM-Chem models.

2 Nocturnal iodine radical activation mechanism

We use the reaction mechanism that has recently been described in the global modelling studies by Saiz-Lopez et al. (2014) and Ordóñez et al. (2012) (see Supplement). In addition to the reactions included in that scheme, we also include nighttime gas-phase reactions based on the theoretical calculations described below. The additional reactions are listed in Table 1, and a scheme with this new nocturnal chemistry is included in Fig. 1.

To the best of our knowledge, reactions of HOI specific to nighttime have not been studied, either theoretically or through laboratory experiments. Currently, HOI is thought to build up overnight until sunrise, with only heterogeneous uptake on sea-salt aerosol as a nighttime loss process (Saiz-Lopez et al., 2012b; Simpson et al., 2015). In addition to the well known

$$I_2 + NO_3 \rightarrow I + IONO_2 \quad \text{(R1)}$$

(Chambers et al., 1992), here we consider several possible HOI reactions that could occur at night, in the absence of photolysis and OH:

$$HOI + NO_2 \rightarrow I + HNO_3 \quad \text{(R2)}$$
$$HOI + HNO_3 \rightarrow IONO_2 + H_2O \quad \text{(R3)}$$
$$HOI + NO_3 \rightarrow IO + HNO_3. \quad \text{(R4)}$$

3 Theoretical calculations

In order to explore the feasibility of Reactions (R2)–(R4) taking place under the conditions of the lower troposphere, we carried out electronic structure calculations using the hybrid density functional/Hartree–Fock B3LYP method from within the Gaussian 09 suite of programs (Frisch et al., 2009), combined with a G2 level basis set for I (Glukhovtsev et al., 1995)

Table 1. Nighttime reactions of emitted inorganic iodine compounds considered in addition to the iodine chemistry scheme used by Saiz-Lopez et al. (2014).

No.	Reaction	Notes
Reaction (R1)	$I_2 + NO_3 \rightarrow I + IONO_2$	1.5×10^{-12} cm^3 molecule^{-1} s^{-1} (Chambers et al., 1992).
Reaction (R2)	$HOI + NO_2 \rightarrow I + HNO_3$	Endothermic by 9 kJ mol^{-1} and the transition state is 73 kJ mol^{-1} above the reactants.
Reaction (R3)	$HOI + HNO_3 \rightarrow IONO_2 + H_2O$	Exothermic by 11 kJ mol^{-1}. The reaction first forms a complex 21 kJ mol^{-1} below the reactants, but this rearranges to the products via a transition state that is 110 kJ mol^{-1} above the reactants.
Reaction (R4)	$HOI + NO_3 \rightarrow IO + HNO_3$	Exothermic by 11 kJ mol^{-1} with all transition states below the reactants. $k(T) = 2.7 \times 10^{-12}\ (300\ \mathrm{K}/T)^{2.66}$ cm^3 molecule^{-1} s^{-1}.

and the standard 6–311 + g(2d,p) triple-zeta basis set for O, N and H. Following geometry optimizations of the relevant points on the potential energy surfaces, and the determination of their corresponding vibrational frequencies and (harmonic) zero-point energies, energies relative to the reactants were obtained at the same level of theory. Spin–orbit corrections of −30.0 (Mečiarová et al., 2011), −14.4 (Khanniche et al., 2016), −5.9 (Šulková et al., 2013) and −4.8 (Kaltsoyannis and Plane, 2008) kJ mol^{-1} were applied to the energies of I, IO, HOI and $IONO_2$, respectively.

Reaction (R2) is endothermic by 2.6 kJ mol^{-1}, and therefore within the expected error of ±10 kJ mol^{-1} at this level of theory. Hence, it might be reasonably fast. However, the transition state of the reaction, which is illustrated in Fig. 2a, is 73 kJ mol^{-1} above the reactants, so this reaction will not occur at tropospheric temperatures. Reaction (R3) is exothermic by 19.8 kJ mol^{-1}. An HOI–HNO_3 complex first forms (Fig. 2b), which is 21 kJ mol^{-1} below the reactants. However, this complex re-arranges to the $IONO_2 + H_2O$ products via the cyclic transition state shown in Fig. 2c, which is 110 kJ mol^{-1} above the reactants.

The stationary points on the potential energy surface (PES) for Reaction (R4) are illustrated in Fig. 3. HOI and NO_3 associate to form a complex which is 24 kJ mol^{-1} below the reactant entrance channel. Hydrogen atom transfer involves a submerged transition state to form an IO–HNO_3 complex, which can then dissociate to the products $IO + HNO_3$. The vibrational frequencies, rotational energies and geometries (in Cartesian co-ordinates) of these intermediates are listed in Table 2. Overall, the reaction is exothermic by 14 kJ mol^{-1}. The energies of the HOI–NO_3 complex and the transition state are assigned the same spin–orbit correction as HOI (−5.9 kJ mol^{-1}; Šulková et al., 2013), whereas the IO–HNO_3 complex is assigned the spin–orbit correction of IO (−14.4 kJ mol^{-1}; Khanniche et al., 2016). This reflects the H–OI bond only increasing from 0.97 Å in HOI to 1.1 Å in the transition state, compared with 1.7 Å in the IO–HNO_3 complex. The spin–orbit correction for the transition state is therefore likely to be closer to that of HOI. Assigning the HOI spin–orbit correction therefore means that the barrier is highest with respect to the reactants so that the estimated rate coefficient (see below) may be a lower limit.

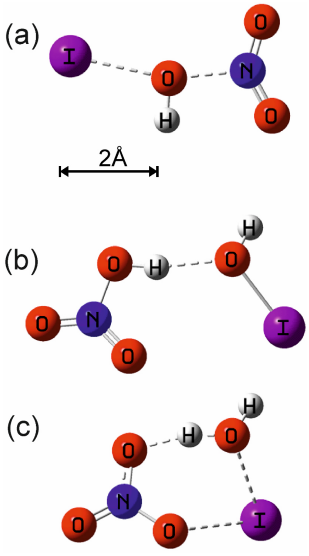

Figure 2. (a) Transition state for the reaction between HOI and NO_2 to form $HNO_3 + I$ and **(b)** complex formed between HOI and HNO_3, which then reacts via transition state **(c)** to form $IONO_2 + H_2O$.

The rate coefficient for Reaction (R4) was then estimated using Rice–Ramsperger–Kassel–Markus (RRKM) theory, employing a multi-well energy-grained master equation solver based on the inverse Laplace transform method – MESMER (Master Equation Solver for Multi-well Energy Reactions) (Roberston et al., 2014). The reaction proceeds via the formation of the excited HOI–NO_3 complex from $HOI + NO_3$. This complex can then dissociate back to the reactants or rearrange to the IO–HNO_3 intermediate complex over the transition state, which can in turn dissociate to the products $IO + HNO_3$. Either of the intermediates can also be stabilized by collision with the third body (N_2). The time evolution of all these possible outcomes is modelled using the master equation.

Table 2. Calculated vibrational frequencies, rotational constants and energies of the stationary points and asymptotes on the $HOI + NO_3$ doublet potential energy surface.

Species	Geometry[a]	Vibrational frequencies[b]	Rotational constants[c]	Potential energy[d]
$HOI + NO_3$		603, 1084, 3803 and 261, 261, 805,1108, 1108, 1126	623.9, 8.182, 8.076 and 13.84, 13.84, 6.919	0.0
IOH–NO_3 complex	O 1.623, 0.284, −0.331 H 1.484, −0.657, −0.043 I 0.009, 1.205, 0.286 N −0.456, −2.265, 0.030 O −1.052, −3.321, −0.0473 O −1.147, −1.195, −0.228 O 0.742, −2.161, 0.333	55, 84, 118, 161, 196, 615, 629, 667, 705, 803, 968, 1228, 1273,1491, 3268	5.610, 0.916, 0.806	−24.0
IO–H–NO_2 TS	O 0.309, 1.515, 0.247 H −0.834, 1.314, −0.017 I 1.280, −0.089, −0.093 N −2.349, −0.133, 0.019 O −3.518, −0.429, −0.035 O −1.444, −0.962, 0.257 O −2.019, 1.117, −0.187	1249*i*, 70, 97, 103, 225, 472, 676, 698, 797, 806, 1041, 1147, 1308, 1513, 1626	6.300, 0.864, 0.767	−16.4
IO–HNO_3 complex	O 0.571, 1.350, 0.348 H −1.111, 1.098, −0.020 I 1.870, 0.0645, −0.152 N −2.503, −0.202, 0.0186 O −3.673, −0.396, −0.170 O −1.654, −0.986, 0.401 O −2.081, 1.090, −0.242	35, 43, 76, 126, 198, 623, 677, 703, 772, 798, 939, 1331, 1416, 1713, 3281	7.058, 0.605, 0.566	−34.8
$IO + HNO_3$		648 and 477, 585, 649, 782, 901, 1320, 1345, 1738, 3724	9.844 and 13.01, 12.05, 6.258	−10.6

[a] Cartesian co-ordinates in Å. [b] Given as wavenumber in cm^{-1}. [c] In GHz. [d] In kJ mol^{-1}, including zero-point energy and spin–orbit coupling of I and IO (see text).

The internal energies of the intermediates on the PES were divided into a contiguous set of grains (width 10 cm^1), each containing a bundle of rovibrational states calculated with the molecular parameters in Table 2, using the rigid-rotor harmonic oscillator approximation for all species. It should be noted that the HOI–NO_3 and IO–HNO_3 complexes both have low-frequency vibrational modes (< 100 cm^{-1}) which should more correctly be treated as hindered rotors rather than vibrations. However, in our experience this is not worth doing this until experimental rate coefficients are available to fit the rotor barrier heights. In any case, the energies of both complexes are far enough below the energy of the entrance channel (Fig. 3) that relatively small changes in their densities of states will have a minor effect on the overall rate coefficient. Each grain was then assigned a set of microcanonical rate coefficients linking it to other intermediates, calculated by RRKM theory. For dissociation to products or reactants, microcanonical rate coefficients were determined using inverse Laplace transformation to link them directly to the capture rate coefficient, $k_{capture}$. For Reaction (R4) and the reverse reaction $IO + HNO_3$ involving neutral species, $k_{capture}$ was set to a typical capture rate coefficient of 2.5×10^{-10} $(T/300\,K)^{1/6}$ cm^3 $molecule^{-1}$ s^{-1}, where the small positive temperature dependence is characteristic of a long-range potential governed by dispersion and dipole–dipole forces (Georgievskii and Klippenstein, 2005).

The probability of collisional transfer between grains was estimated using the exponential down model, where the average energy for downward transitions was set to $<\Delta E>_{down} = 300\,cm^{-1}$ for N_2 as the third body (Gilbert and Smith, 1990). MESMER determines the temperature- and pressure-dependent rate coefficient from the full microcanonical description of the system time evolution by performing an eigenvector/eigenvalue analysis (Bartis and Widom, 1974). The resulting rate coefficient over the temperature range 260–300 K at a pressure of 1000 hPa is

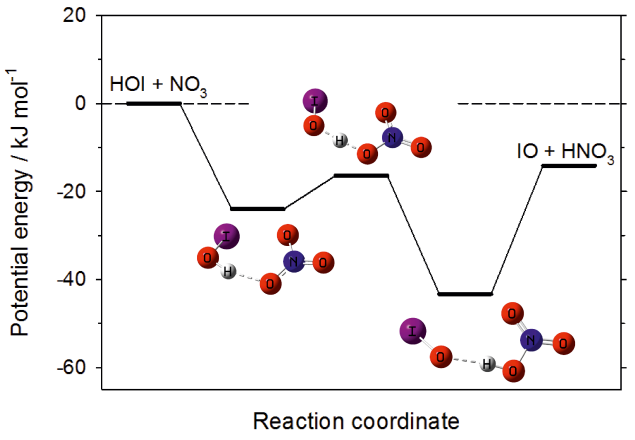

Figure 3. Potential energy surface for the reaction between HOI and NO_3, which contains two intermediate complexes separated by a submerged barrier.

$k_4(T) = 2.7 \times 10^{-12}\,(300\,\mathrm{K}/T)^{2.66}\,\mathrm{cm^3\ molecule^{-1}\ s^{-1}}$. Because the intermediate complexes are not strongly bound, and the transition state and products are below the entrance channel, the only products formed in Reaction (R4) under atmospheric conditions are $IO + HNO_3$. The uncertainty in k_4 arises principally from the estimated capture rate coefficient (see above) and the height of the barrier below the entrance channel. As discussed above, the spin–orbit correction of the transition state is likely to be larger than the value of $-5.9\,\mathrm{kJ\,mol^{-1}}$ corresponding to HOI, so k_4 is possibly a lower limit. For instance, if the barrier height is decreased by $3\,\mathrm{kJ\,mol^{-1}}$, k_4 increases by a factor of 1.9. If the barrier is lower by $8.5\,\mathrm{kJ\,mol^{-1}}$ (corresponding to the transition state having the same spin–orbit correction as IO), then k_4 would increase by a factor of 5.1. Nevertheless, noting that the capture rate coefficient could be lower – perhaps by a factor of 2 – than the estimate used here, we prefer to use the value for k_4 calculated with the potential surface in Fig. 3. Of course, if k_4 is larger, then the atmospheric impacts of Reaction (R4) discussed in Sect. 4 will be even more pronounced.

Note that NO_3 also reacts with CH_2I_2 with a rate constant $\sim 2\text{–}4 \times 10^{-13}\,\mathrm{cm^3\ molecule^{-1}\ s^{-1}}$, which can have a significant effect on nighttime CH_2I_2 concentration (Carpenter et al., 2015). However the products of this reaction are still uncertain (Nakano et al., 2006; Carpenter et al., 2015) and its rate is considerably slower than that of Reaction (R4).

In summary, the only likely gas-phase reactions that I_2 and HOI undergo in the nighttime troposphere are Reactions (R1) and (R4), respectively. These are included in the model reaction scheme to examine their impacts on the evolution of iodine species in the atmosphere.

4 Atmospheric modelling

We use two atmospheric chemical transport models to study (i) the impact of this new chemistry on the nighttime chemistry and partitioning of iodine species and (ii) the resulting geographical distribution of nocturnal iodine and impact on NO_3 within the global marine boundary layer.

The first model, Tropospheric HAlogen chemistry MOdel (THAMO) (Saiz-Lopez et al., 2008), is used for a detailed kinetics study of the impact of the different reactions shown in Table 1 as well as to assess which uptake rates best reproduce observations from a field study at the CVAO (Carpenter et al., 2011). THAMO has been used in the past to study iodine chemistry at the CVAO, and further details including the full chemical scheme can be found elsewhere (Saiz-Lopez et al., 2008; Mahajan et al., 2009, 2010a, b; Lawler et al., 2014). Briefly, THAMO is a 1-D chemistry transport model with 200 stacked boxes at a vertical resolution of 5 m (total height 1 km). The model treats iodine, bromine, O_3, NO_x and HO_x chemistry and is constrained with typical measured values of other chemical species in the MBL: $[CO] = 110\,\mathrm{nmol\,mol^{-1}}$; $[DMS] = 30\,\mathrm{pmol\,mol^{-1}}$; $[CH_4] = 1820\,\mathrm{nmol\,mol^{-1}}$; [ethane] $= 925\,\mathrm{pmol\,mol^{-1}}$; $[CH_3CHO] = 970\,\mathrm{pmol\,mol^{-1}}$; $[HCHO] = 500\,\mathrm{pmol\,mol^{-1}}$; [isoprene] $= 10\,\mathrm{pmol\,mol^{-1}}$; [propane] $= 60\,\mathrm{pmol\,mol^{-1}}$; [propene] $= 20\,\mathrm{pmol\,mol^{-1}}$. The average background aerosol surface area (ASA) used is $1 \times 10^{-6}\,\mathrm{cm^2\,cm^{-3}}$ (Read et al., 2008, 2009; Lee et al., 2009, 2010). The model is initialized at midnight and the evolution of iodine species, O_3, NO_x and HO_x is followed until the model reaches steady state.

The second model is the global 3-D chemistry-climate model CAM-Chem (Community Atmospheric Model with chemistry, version 4.0), which is used to study the impact of Reaction (R1) and (R4) on a global scale. The model includes a comprehensive chemistry scheme to simulate the evolution of trace gases and aerosols in the troposphere and the stratosphere (Lamarque et al., 2012). The model runs with the iodine, bromine and chlorine chemistry schemes from previous studies (Fernandez et al., 2014; Saiz-Lopez et al., 2014, 2015), including the photochemical breakdown of bromo- and iodocarbons emitted from the oceans (Ordóñez et al., 2012) and abiotic oceanic sources of HOI and I_2 (Prados-Roman et al., 2015a). CAM-Chem has been configured in this work with a horizontal resolution of 1.9° latitude by 2.5° longitude and 26 vertical levels, from the surface to ~ 40 km altitude. All model runs in this study were performed in the specified dynamics mode (Lamarque et al., 2012) using offline meteorological fields instead of an online calculation, to allow direct comparisons between different simulations. This offline meteorology consists of a high-frequency meteorological input from a previous free running climatic simulation.

It should be noted that during nighttime the uptake on aerosols of emitted species such as I_2 and HOI, and the uptake of reservoir species such as $IONO_2$, can play a major

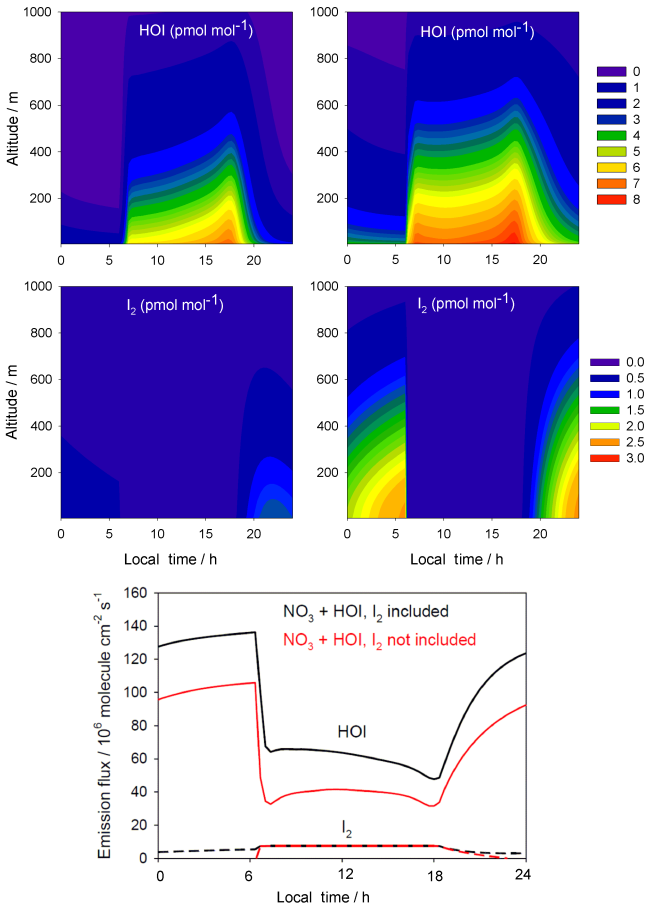

Figure 4. THAMO modelled diurnal variation of HOI, I_2 (upper panels) and the HOI / I_2 flux from the ocean surface (bottom panel). The right-hand panels are from Scenario 1, which do not include nighttime reactions of HOI and I_2 with NO_3, while the left-hand panels include the reactions in Scenario 2. In bottom panel red lines represent Scenario 1, while black lines correspond to Scenario 2.

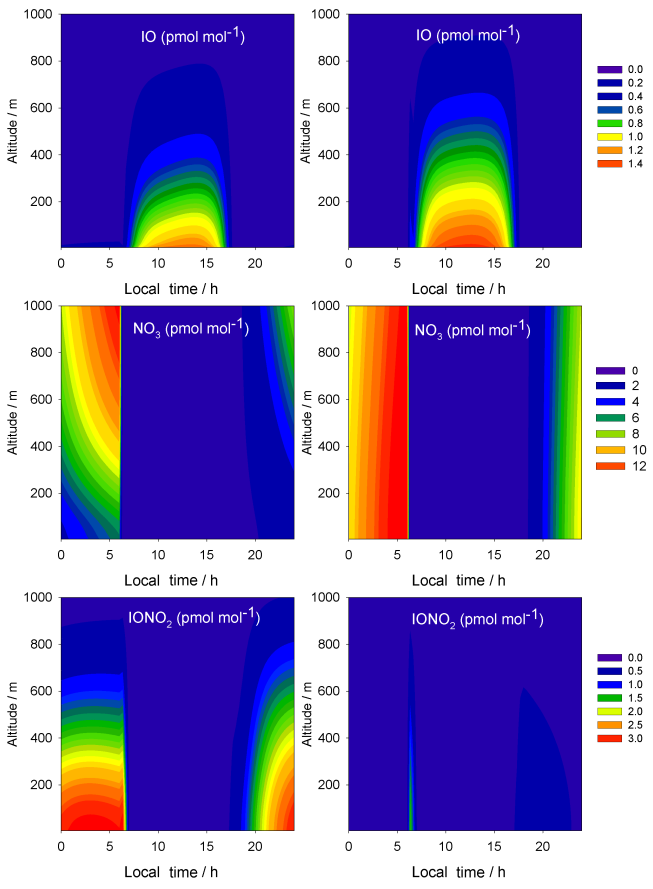

Figure 5. THAMO modelled diurnal variation of IO, NO_3 and the $IONO_2$. The right-hand panels are from Scenario 1, which do not include nighttime reactions of HOI and I_2 with NO_3, while the left-hand panels include the reactions in Scenario 2.

role in the cycling of iodine. Observations at CVAO show that I_2 peaked at about 1 pmol mol^{-1} during the night and that ICl was not detected above the 1 pmol mol^{-1} detection limit of the instrument (Lawler et al., 2014). In order to match these observations, we need to reduce the uptake and heterogeneous recycling of iodine species. The uptake rates of chemical species on the background sea-salt aerosols are determined by their uptake coefficients (γ). The database of mass accommodation and/or uptake coefficients is rather sparse and essentially limited to I_2, HI, HOI, ICI and IBr on pure water/ice and on sulfuric acid particles (Sander et al., 2006). Other iodine species which are likely to undergo uptake onto aerosol are OIO, HIO_3, INO_2, $IONO_2$ and I_2O_2 (Saiz-Lopez et al., 2012a; Sommariva et al., 2012). Uptake of HOI is very uncertain, with γ(HOI) ranging from 2×10^{-3} to 0.3 depending on the surface composition and state (Holmes et al., 2001). Sommariva et al. (2012) assumed γ(HOI) to be 0.6, similar to the value for HOBr measured by Wachsmuth et al. (2002). In the case of $IONO_2$, the uptake coefficient has not been measured, with most models using values of 0.1 (von Glasow et al., 2002; Saiz-Lopez et al., 2008; Mahajan et al., 2009, 2010a, b; Leigh et al., 2010; Sommariva et al., 2012; Lawler et al., 2014). The modelled levels of I_2 and ICl change with different values of uptake coefficients. To match the CVAO I_2 and ICl observations (Lawler et al., 2014), we have used $\gamma = 0.01$ for HOI and $IONO_2$, which is within the uncertainty in the literature, and assumed that 80 % is recycled as I_2. Further measurements of these dihalogen species are needed to better constrain their heterogeneous recycling on sea-salt aerosols.

5 Results and discussion

Of the possible nocturnal iodine activation reactions involving the inorganic iodine source gases I_2 and HOI, only Reactions (R1) and (R4) appear to be likely candidates (see Sect. 3). We therefore designed two modelling scenarios: Scenario 1 (S1), without nighttime reactions of I_2 or HOI

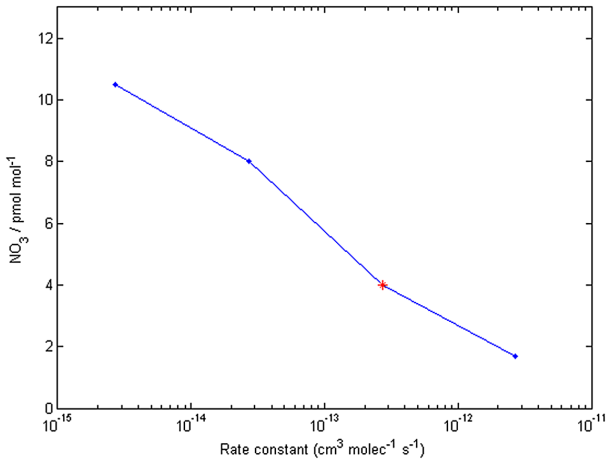

Figure 6. Sensitivity run showing the effect of the uncertainty in the rate constant estimation on the reduction of NO_3 peak nighttime concentration at the surface – the red point is the theoretical estimate.

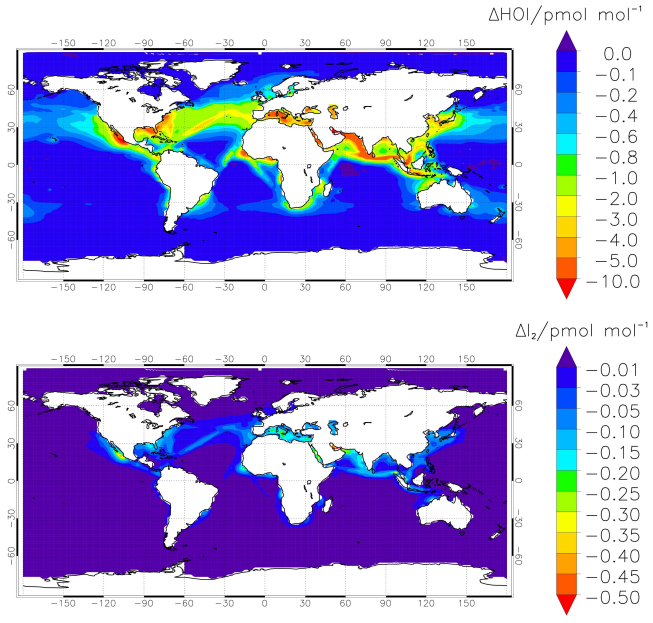

Figure 7. Modelled annual average of HOI **(a)** and I_2 **(b)** during nighttime (from 00:00 to 01:00 LT) at the surface level. The panels show the difference in volume mixing ratio between the simulations with and without Reactions (R1) and (R4).

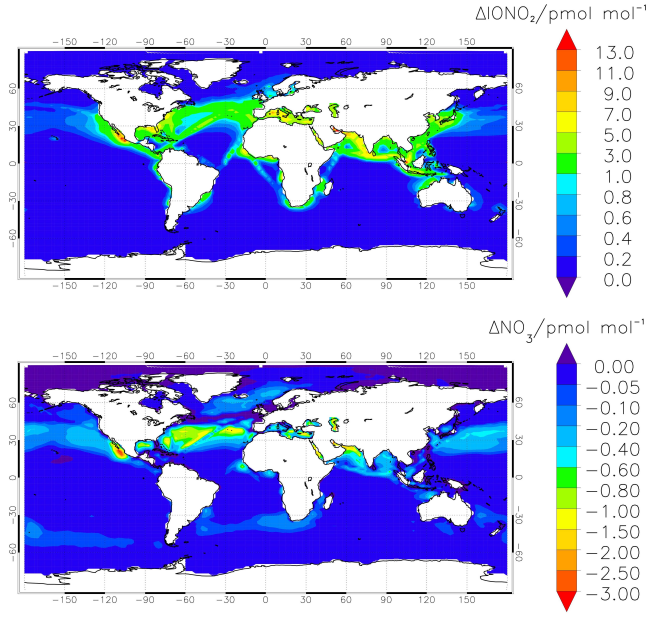

Figure 8. Modelled annual average of $IONO_2$ **(a)** and NO_3 **(b)** during nighttime (from 00:00 to 01:00 LT) at the surface level, as the difference in volume mixing ratio between the simulations with and without Reactions (R1) and (R4).

with NO_3; and Scenario 2 (S2), including Reactions (R1) and (R4) for the degradation of HOI and I_2 by NO_3. In the one-dimensional model THAMO, the I_2 and HOI are injected into the atmosphere from the ocean surface using the flux parameterizations derived from laboratory experiments (Carpenter et al., 2013; MacDonald et al., 2014). Figure 4 shows the resulting diurnal evolution of the HOI and I_2 mixing ratios in the two scenarios, after 2 days of simulation time. The I_2 mixing ratio peaks during the night in both the scenarios due to quick loss by photolysis during the daytime. By contrast, HOI is present during daytime due to its production through the reaction of IO with HO_2 and peaks just before sunset. In the first scenario, without the inclusion of Reactions (R1) and (R4), Fig. 4 (panels on right-hand side) shows that I_2 builds up during the night, reaching a concentration peak just before dawn. This is especially noticeable as the daytime concentrations are much lower than during the night. On the other hand, HOI concentrations decrease during night until dawn, when they drop to zero. For both species, inclusion of reactions with NO_3 causes a decrease in their respective nocturnal concentrations (Fig. 4, panels on left-hand side). The inclusion of Reactions (R1) and (R4) also leads to a modelled I_2 concentration which is in better agreement with the observations of the molecule made at CVAO (Lawler et al., 2014), reaching peak values of about 1 pmol mol^{-1}, as compared to about 3 pmol mol^{-1} for the scenario without nighttime reactions. An additional consequence of including Reactions (R1) and (R4) is the significant increase of the sea–air fluxes of HOI and I_2 at night due to their atmospheric removal by NO_3 (Fig. 4, bottom panel).

Figure 5 shows the diurnal evolution of IO, NO_3 and $IONO_2$ in both model scenarios after 2 days of simulation time. Although the daytime peak values of IO are well reproduced in both scenarios, reaching about 1.5 pmol mol^{-1} around noon similar to the ground-based observations (Read et al., 2008), the inclusion of Reactions (R1) and (R4) leads to the removal of the dawn spike in IO, which is predicted by current iodine models but was not observed at CVAO

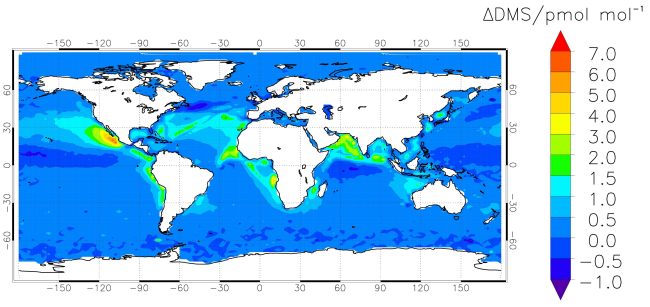

Figure 9. Increase in the DMS levels during nighttime (from 00:00 to 01:00 LT) at the surface level due to the inclusion of the Reactions (R1) and (R4) in CAM-Chem.

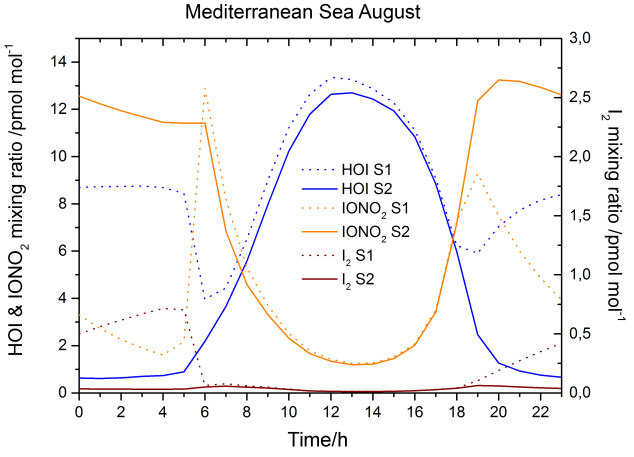

Figure 10. Hourly averaged concentration of HOI, $IONO_2$ and I_2 in the Mediterranean Sea at the surface level (long: 10 → 20° E, lat: 33 → 40° N)

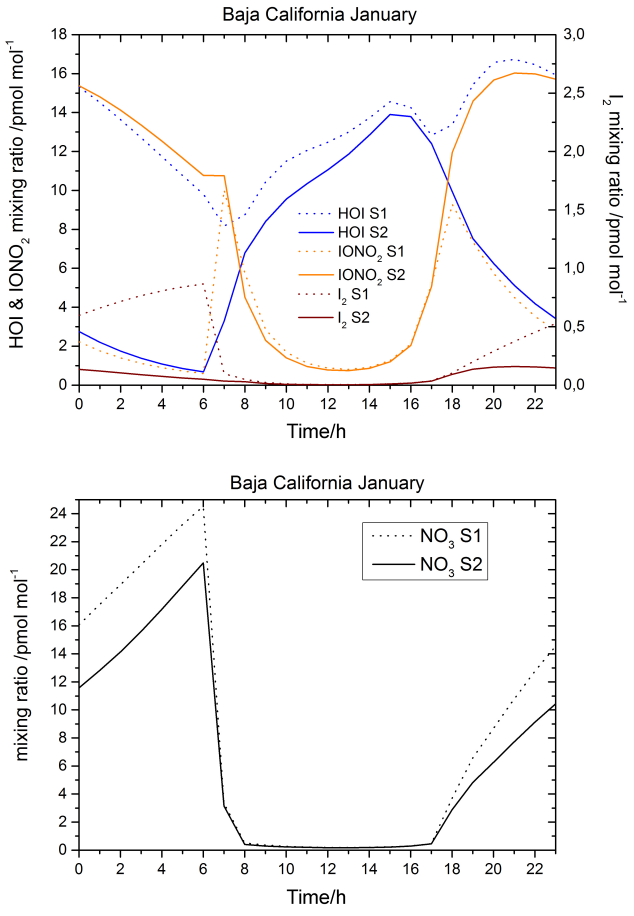

Figure 11. Hourly averaged concentration of HOI, $IONO_2$ and I_2 (upper panel) and NO_3 (bottom panel) in the Pacific Ocean at the south of Baja California Peninsula at the surface level (long: −110 → −106° E, lat: 16 → 23° N)

(Read et al., 2008; Mahajan et al., 2010a). The IO dawn spike predicted by models is due to a buildup of the emitted I_2 and HOI (which is converted into IBr / ICl through heterogeneous recycling) over the night, followed by rapid photolysis after first sunlight. However, due to the considerable removal of HOI and I_2 through the night due to reaction with ambient NO_3, this spike does not appear in the second scenario, leading to a modification of the diurnal profile of IO that better matches with observations.

Reactions (R1) and (R4) also reduce the NO_3 mixing ratio (Fig. 5, middle panels). In Scenario 1, the NO_3 is modelled to peak at about 14 pmol mol^{-1} just before dawn. However, the inclusion of Reactions (R1) and (R4) leads to near complete depletion of NO_3 close to the surface, with the peak level at the surface reaching only 2 pmol mol^{-1}, since Reactions (R1) and (R4) become the main atmospheric loss processes for NO_3 in the lower MBL. These reactions lead however to the buildup of $IONO_2$ during the night (Fig. 5, bottom panels). In the absence of Reactions (R1) and (R4), significant levels of $IONO_2$ are seen only at dawn and dusk since no other reactions produce $IONO_2$ at night, and during the day $IONO_2$ is removed by photolysis. However, with continuous conversion of I_2 and HOI to $IONO_2$ by Reactions (R1) and (R4) in Scenario 2, $IONO_2$ is modelled to reach up to 3 pmol mol^{-1} in the nocturnal MBL.

Given the associated uncertainty in the theoretical estimate of the k_4, we used THAMO to assess the sensitivity of surface NO_3 to k_4. Figure 6 shows that NO_3 peak nighttime concentration is in fact highly coupled to k_4, with the expected uncertainty in k_4 of 1 order of magnitude (see above) giving rise to a factor-of-2 change in NO_3. A laboratory measurement of k_4 should therefore be undertaken in the future.

We now implement the nighttime reactions in the 3-D global model (CAM-Chem) to assess the resulting geographical distributions and impacts of these reactions. We have also run two different scenarios in CAM-Chem, the first without Reactions (R1) and (R4) in the chemical scheme, and the second including the new nighttime iodine chemistry. Figure 7 shows how the inclusion of Reactions (R1) and (R4) reduces globally the nighttime concentrations of I_2 and HOI. The plots correspond to the nighttime averaged

(from 00:00 to 01:00 LT (local time)) differences between the model scenarios. Considerable reductions of up to 0.5 and 10 pmol mol^{-1} (i.e. up to 100 % removal) are observed for I_2 and HOI, respectively, particularly over coastal polluted regions where continental pollution outflow leads to higher levels of NO_3 in the nighttime MBL. Major shipping routes also show strong nocturnal iodine activity due to the characteristically high NO_x, and resulting NO_3, associated with shipping emissions.

Figure 8 shows the effect of this nocturnal chemistry on the concentrations of $IONO_2$ and NO_3. As in the previous figure, the plots correspond to the nighttime averaged difference between the second and the first scenarios. The maps show an increase of $IONO_2$ of up to 15 pmol mol^{-1} ($\sim$ 600 %) over polluted coastal areas, due to efficient conversion of NO_3 into $IONO_2$. The bottom panel of Figure 7 shows the expected decrease of NO_3 levels associated with the inclusion of Reactions (R1) and (R4), with decreases of up to $\sim$ 4 pmol mol^{-1} (up to 60 %) over marine polluted regions. We model global percentage reductions in the NO_3 concentrations of 7.1 % (60° S–60° N), with nitrate removal of up to 80 % in non-polluted remote oceanic regions with low NO_3 levels. This in turn can affect the modelled oxidation of DMS by NO_3. We estimate that the reduction in NO_3, due to the inclusion of Reactions (R1) and (R4), results in a model increase in DMS levels of up to 7 pmol mol^{-1} (about 20 %) in marine regions affected by continental pollution outflow (Fig. 9). We therefore suggest that the inclusion of the new nighttime iodine chemistry can have a large, so far unrecognized, impact on the nocturnal oxidizing capacity of the marine atmosphere.

The hourly evolution of the main species involved in this study is shown in Figs. 10 and 11, which include the levels of HOI, I_2, $IONO_2$ and NO_3 in the MBL over regions where nocturnal iodine is modelled to be particularly active. The first region is located within the Mediterranean Sea, an area that shows large differences during the summer months when high ozone levels drive large emissions of HOI and I_2 from the sea, and the high levels of NO_3 at nighttime make this chemistry especially important. The hourly average in August is shown in Fig. 10 for HOI, $IONO_2$ and I_2. HOI and $IONO_2$ (Fig. 10) are the species whose concentration differ most between scenarios as HOI is removed and $IONO_2$ produced by Reaction (R4) (and, to a lesser extent, Reaction R1). Over the Pacific Ocean at the south of the Baja California Peninsula, the modelled differences between the two scenarios are even higher than over the Mediterranean Sea (Fig. 11). Large differences in MBL NO_3, up to 28 %, are modelled during the night caused by pollution outflow from the west coasts of Mexico and USA.

6 Summary and conclusions

The viability of the reaction of HOI with NO_2, HNO_3 and NO_3 has been studied by theoretical calculations. The results indicate that only the reaction of HOI with NO_3, to yield $IO + HNO_3$, is possible under tropospheric conditions. The inclusion of this reaction, along with that of $I_2 + NO_3$, has a number of significant implications:

- Nocturnal iodine radical chemistry is activated.
- This causes enhanced nighttime oceanic emissions of HOI and I_2.
- Nighttime iodine species are partitioned into high levels of $IONO_2$.
- The IO spike, modelled by current iodine models but not shown by observations, is removed.
- A reduction of the levels of nitrate radical in the MBL, with the associated less efficient oxidation of DMS, has important implications for our understanding of the nocturnal oxidizing capacity of the marine atmosphere.

7 Data availability

Data are available upon request to the corresponding author.

The Supplement related to this article is available online at doi:10.5194/acp-16-15593-2016-supplement.

Acknowledgements. This work was supported by the Spanish National Research Council (CSIC). The National Center for Atmospheric Research (NCAR) is funded by the National Science Foundation (NSF). The Climate Simulation Laboratory at NCAR's Computational and Information Systems Laboratory (CISL) provided the computing resources (ark:/85065/d7wd3xhc). As part of the CESM project, CAM-Chem is supported by the NSF and the Office of Science (BER) of the US Department of Energy. This work was also sponsored by the NASA Atmospheric Composition Modeling and Analysis Program (ACMAP, number NNX11AH90G).

Edited by: J.-U. Grooß
Reviewed by: H. K. Roscoe, F. Louis, and two anonymous referees

References

Allan, B. J., McFiggans, G., Plane, J. M. C., Coe, H., and McFadyen, G. G.: The nitrate radical in the remote marine boundary layer, J. Geophys. Res.-Atmos., 105, 24191–24204, doi:10.1029/2000jd900314, 2000.

Allan, J. D., Williams, P. I., Najera, J., Whitehead, J. D., Flynn, M. J., Taylor, J. W., Liu, D., Darbyshire, E., Carpenter, L. J., Chance, R., Andrews, S. J., Hackenberg, S. C., and McFiggans, G.: Iodine observed in new particle formation events in the Arctic atmosphere during ACCACIA, Atmos. Chem. Phys., 15, 5599–5609, doi:10.5194/acp-15-5599-2015, 2015.

Bartis, J. T. and Widom, B.: Stochastic models of the interconversion of three or more chemical species, J. Chem. Phys., 60, 3474–3482, doi:10.1063/1.1681562, 1974.

Butler, J. H., King, D. B., Lobert, J. M., Montzka, S. A., Yvon-Lewis, S. A., Hall, B. D., Warwick, N. J., Mondeel, D. J., Aydin, M., and Elkins, J. W.: Oceanic distributions and emissions of short-lived halocarbons, Global Biogeochem. Cy., 21, GB1023, doi:10.1029/2006gb002732, 2007.

Carpenter, L. J.: Iodine In the marine Boundary Layer, Chem. Rev., 103, 4953–4962, 2003.

Carpenter, L. J., Fleming, Z. L., Read, K. A., Lee, J. D., Moller, S. J., Hopkins, J. R., Purvis, R. M., Lewis, A. C., Müller, K., Heinold, B., Herrmann, H., Fomba, K. W., Pinxteren, D., Müller, C., Tegen, I., Wiedensohler, A., Müller, T., Niedermeier, N., Achterberg, E. P., Patey, M. D., Kozlova, E. A., Heimann, M., Heard, D. E., Plane, J. M. C., Mahajan, A., Oetjen, H., Ingham, T., Stone, D., Whalley, L. K., Evans, M. J., Pilling, M. J., Leigh, R. J., Monks, P. S., Karunaharan, A., Vaughan, S., Arnold, S. R., Tschritter, J., Pöhler, D., Frieß, U., Holla, R., Mendes, L. M., Lopez, H., Faria, B., Manning, A. J., and Wallace, D. W. R.: Seasonal characteristics of tropical marine boundary layer air measured at the Cape Verde Atmospheric Observatory, J. Atmos. Chem., 67, 87–140, doi:10.1007/s10874-011-9206-1, 2011.

Carpenter, L. J., MacDonald, S. M., Shaw, M. D., Kumar, R., Saunders, R. W., Parthipan, R., Wilson, J., and Plane, J. M. C.: Atmospheric iodine levels influenced by sea surface emissions of inorganic iodine, Nat. Geosci., 6, 108–111, doi:10.1038/ngeo1687, 2013.

Carpenter, L. J., Andrews, S. J., Lidster, R. T., Saiz-Lopez, A., Fernandez-Sanchez, M., Bloss, W. J., Ouyang, B., and Jones, R. L.: A nocturnal atmospheric loss of CH_2I_2 in the remote marine boundary layer, J. Atmos. Chem., doi:10.1007/s10874-015-9320-6, 2015.

Chambers, R. M., Heard, A. C., and Wayne, R. P.: Inorganic gas-phase reactions of the nitrate radical: iodine + nitrate radical and iodine atom + nitrate radical, J. Phys. Chem., 96, 3321–3331, doi:10.1021/j100187a028, 1992.

Fernandez, R. P., Salawitch, R. J., Kinnison, D. E., Lamarque, J.-F., and Saiz-Lopez, A.: Bromine partitioning in the tropical tropopause layer: implications for stratospheric injection, Atmos. Chem. Phys., 14, 13391–13410, doi:10.5194/acp-14-13391-2014, 2014.

Frisch, M., Trucks, G., Schlegel, H., Scuseria, G., Robb, M., Cheeseman, J., Scalmani, G., Barone, V., Mennucci, B., and Petersson, G.: Gaussian 09, Revision A. 1., Wallingford, CT: Gaussian, Inc, 2009.

Georgievskii, Y. and Klippenstein, S. J.: Long-range transition state theory, J. Chem. Phys., 122, 194103, doi:10.1063/1.1899603, 2005.

Gilbert, R. G. and Smith, S. C.: Theory of Unimolecular and Recombination Reactions, Blackwell, Oxford, 1990.

Glukhovtsev, M. N., Pross, A., McGrath, M. P., and Radom, L.: Extension of Gaussian-2 (G2) theory to bromine- and iodine-containing molecules: Use of effective core potentials, J. Chem. Phys., 103, 1878–1885, 1995.

Gómez Martín, J. C., Galvez, O., Baeza-Romero, M. T., Ingham, T., Plane, J. M. C., and Blitz, M. A.: On the mechanism of iodine oxide particle formation, Phys. Chem. Chem. Phys., 15, 15612–15622, doi:10.1039/c3cp51217g, 2013.

Gómez Martín, J. C., Mahajan, A. S., Hay, T. D., Prados-Román, C., Ordóñez, C., MacDonald, S. M., Plane, J. M. C., Sorribas, M., Gil, M., Paredes Mora, J. F., Agama Reyes, M. V., Oram, D. E., Leedham, E., and Saiz-Lopez, A.: Iodine chemistry in the eastern Pacific marine boundary layer, J. Geophys. Res.-Atmos., 118, 887–904, doi:10.1002/jgrd.50132, 2013.

Großmann, K., Frieß, U., Peters, E., Wittrock, F., Lampel, J., Yilmaz, S., Tschritter, J., Sommariva, R., von Glasow, R., Quack, B., Krüger, K., Pfeilsticker, K., and Platt, U.: Iodine monoxide in the Western Pacific marine boundary layer, Atmos. Chem. Phys., 13, 3363–3378, doi:10.5194/acp-13-3363-2013, 2013.

Hoffmann, T., O'Dowd, C. D., and Seinfeld, J. H.: Iodine oxide homogeneous nucleation: An explanation for coastal new particle production, Geophys. Res. Lett., 28, 1949–1952, 2001.

Holmes, N. S., Adams, J. W., and Crowley, J. N.: Uptake and reaction of HOI and $IONO_2$ on frozen and dry NaCl / NaBr surfaces and H_2SO_4, Phys. Chem. Chem. Phys., 3, 1679–1687, doi:10.1039/b100247n, 2001.

Jones, C. E., Hornsby, K. E., Sommariva, R., Dunk, R. M., von Glasow, R., McFiggans, G., and Carpenter, L. J.: Quantifying the contribution of marine organic gases to atmospheric iodine, Geophys. Res. Lett., 37, L18804, doi:10.1029/2010GL043990, 2010.

Kaltsoyannis, N. and Plane, J. M. C.: Quantum chemical calculations on a selection of iodine-containing species (IO, OIO, INO_3, $(IO)_2$, I_2O_3, I_2O_4 and I_2O_5) of importance in the atmosphere., Phys. Chem. Chem. Phys., 10, 1723–1733, 2008.

Khanniche, S., Louis, F., Cantrel, L., and Černušák, I.: A Density Functional Theory and ab Initio Investigation of the Oxidation Reaction of CO by IO Radicals, J. Phys. Chem. A, 120, 1737–1749, 2016.

Lamarque, J.-F., Emmons, L. K., Hess, P. G., Kinnison, D. E., Tilmes, S., Vitt, F., Heald, C. L., Holland, E. A., Lauritzen, P. H., Neu, J., Orlando, J. J., Rasch, P. J., and Tyndall, G. K.: CAM-chem: description and evaluation of interactive atmospheric chemistry in the Community Earth System Model, Geosci. Model Dev., 5, 369–411, doi:10.5194/gmd-5-369-2012, 2012.

Lawler, M. J., Mahajan, A. S., Saiz-Lopez, A., and Saltzman, E. S.: Observations of I_2 at a remote marine site, Atmos. Chem. Phys., 14, 2669–2678, doi:10.5194/acp-14-2669-2014, 2014.

Lee, J. D., Moller, S. J., Read, K. A., Lewis, A. C., Mendes, L., and Carpenter, L. J.: Year-round measurements of nitrogen oxides and ozone in the tropical North Atlantic marine boundary layer, J. Geophys. Res.-Atmos., 114, D21302, doi:10.1029/2009jd011878, 2009.

Lee, J. D., McFiggans, G., Allan, J. D., Baker, A. R., Ball, S. M., Benton, A. K., Carpenter, L. J., Commane, R., Finley, B. D., Evans, M., Fuentes, E., Furneaux, K., Goddard, A., Good, N., Hamilton, J. F., Heard, D. E., Herrmann, H., Hollingsworth, A., Hopkins, J. R., Ingham, T., Irwin, M., Jones, C. E., Jones, R. L., Keene, W. C., Lawler, M. J., Lehmann, S., Lewis, A. C., Long, M. S., Mahajan, A., Methven, J., Moller, S. J., Müller, K., Müller, T., Niedermeier, N., O'Doherty, S., Oetjen, H., Plane, J. M. C., Pszenny, A. A. P., Read, K. A., Saiz-Lopez, A., Saltzman, E. S., Sander, R., von Glasow, R., Whalley, L., Wiedensohler, A., and Young, D.: Reactive Halogens in the Marine Boundary Layer (RHaMBLe): the tropical North Atlantic experiments, Atmos. Chem. Phys., 10, 1031–1055, doi:10.5194/acp-10-1031-2010, 2010.

Leigh, R. J., Ball, S. M., Whitehead, J., Leblanc, C., Shillings, A. J. L., Mahajan, A. S., Oetjen, H., Lee, J. D., Jones, C. E., Dorsey, J. R., Gallagher, M., Jones, R. L., Plane, J. M. C., Potin, P., and McFiggans, G.: Measurements and modelling of molecular iodine emissions, transport and photodestruction in the coastal region around Roscoff, Atmos. Chem. Phys., 10, 11823–11838, doi:10.5194/acp-10-11823-2010, 2010.

MacDonald, S. M., Gómez Martín, J. C., Chance, R., Warriner, S., Saiz-Lopez, A., Carpenter, L. J., and Plane, J. M. C.: A laboratory characterisation of inorganic iodine emissions from the sea surface: dependence on oceanic variables and parameterisation for global modelling, Atmos. Chem. Phys., 14, 5841–5852, doi:10.5194/acp-14-5841-2014, 2014.

Mahajan, A. S., Oetjen, H., Saiz-Lopez, A., Lee, J. D., McFiggans, G. B., and Plane, J. M. C.: Reactive iodine species in a semi-polluted environment, Geophys. Res. Lett., 36, L16803, doi:10.1029/2009GL038018, 2009.

Mahajan, A. S., Plane, J. M. C., Oetjen, H., Mendes, L., Saunders, R. W., Saiz-Lopez, A., Jones, C. E., Carpenter, L. J., and McFiggans, G. B.: Measurement and modelling of tropospheric reactive halogen species over the tropical Atlantic Ocean, Atmos. Chem. Phys., 10, 4611–4624, doi:10.5194/acp-10-4611-2010, 2010a.

Mahajan, A. S., Shaw, M., Oetjen, H., Hornsby, K. E., Carpenter, L. J., Kaleschke, L., Tian-Kunze, X., Lee, J. D., Moller, S. J., Edwards, P., Commane, R., Ingham, T., Heard, D. E., and Plane, J. M. C.: Evidence of reactive iodine chemistry in the Arctic boundary layer, J. Geophys. Res.-Atmos., 115, D20303, doi:10.1029/2009JD013665, 2010b.

Mahajan, A. S., Gómez Martín, J. C., Hay, T. D., Royer, S.-J., Yvon-Lewis, S., Liu, Y., Hu, L., Prados-Roman, C., Ordóñez, C., Plane, J. M. C., and Saiz-Lopez, A.: Latitudinal distribution of reactive iodine in the Eastern Pacific and its link to open ocean sources, Atmos. Chem. Phys., 12, 11609–11617, doi:10.5194/acp-12-11609-2012, 2012.

McFiggans, G., Coe, H., Burgess, R., Allan, J., Cubison, M., Alfarra, M. R., Saunders, R., Saiz-Lopez, A., Plane, J. M. C., Wevill, D., Carpenter, L., Rickard, A. R., and Monks, P. S.: Direct evidence for coastal iodine particles from Laminaria macroalgae – linkage to emissions of molecular iodine, Atmos. Chem. Phys., 4, 701–713, doi:10.5194/acp-4-701-2004, 2004.

Mečiarová, K., Šulka, M., Canneaux, S., Louis, F., and Černušáka, I.: A theoretical study of the kinetics of the forward and reverse reactions $HI + CH_3 = I + CH_4$, Chem. Phys. Lett., 517, 149–154, 2011.

Nakano, Y., Ukeguchi, H., and Ishiwata, T.: Rate constant of the reaction of NO_3 with CH_2I_2 measured with use of cavity ring-down spectroscopy, Chem. Phys. Lett., 430, 235–239, doi:10.1016/j.cplett.2006.09.002, 2006.

O'Dowd, C. D., Jimenez, J. L., Bahreini, R., Flagan, R. C., Seinfeld, J. H., Hameri, K., Pirjola, L., Kulmala, M., Jennings, S. G., and Hoffmann, T.: Marine aerosol formation from biogenic iodine emissions, Nature, 417, 632–636, 2002.

Ordóñez, C., Lamarque, J.-F., Tilmes, S., Kinnison, D. E., Atlas, E. L., Blake, D. R., Sousa Santos, G., Brasseur, G., and Saiz-Lopez, A.: Bromine and iodine chemistry in a global chemistry-climate model: description and evaluation of very short-lived oceanic sources, Atmos. Chem. Phys., 12, 1423–1447, doi:10.5194/acp-12-1423-2012, 2012.

Prados-Roman, C., Cuevas, C. A., Fernandez, R. P., Kinnison, D. E., Lamarque, J.-F., and Saiz-Lopez, A.: A negative feedback between anthropogenic ozone pollution and enhanced ocean emissions of iodine, Atmos. Chem. Phys., 15, 2215–2224, doi:10.5194/acp-15-2215-2015, 2015a.

Prados-Roman, C., Cuevas, C. A., Hay, T., Fernandez, R. P., Mahajan, A. S., Royer, S.-J., Galí, M., Simó, R., Dachs, J., Großmann, K., Kinnison, D. E., Lamarque, J.-F., and Saiz-Lopez, A.: Iodine oxide in the global marine boundary layer, Atmos. Chem. Phys., 15, 583–593, doi:10.5194/acp-15-583-2015, 2015b.

Read, K. A., Mahajan, A. S., Carpenter, L. J., Evans, M. J., Faria, B. V. E., Heard, D. E., Hopkins, J. R., Lee, J. D., Moller, S. J., Lewis, A. C., Mendes, L., McQuaid, J. B., Oetjen, H., Saiz-Lopez, A., Pilling, M. J., and Plane, J. M. C.: Extensive halogen-mediated ozone destruction over the tropical Atlantic Ocean, Nature, 453, 1232–1235, 2008.

Read, K. A., Lee, J. D., Lewis, A. C., Moller, S. J., Mendes, L., and Carpenter, L. J.: Intra-annual cycles of NMVOC in the tropical marine boundary layer and their use for interpreting seasonal variability in CO, J. Geophys. Res.-Atmos,, 114, D21303, doi:10.1029/2009jd011879, 2009.

Roberston, S. H., Glowacki, D. R., Liang, C. H., Morley, C., Shannon, R., Blitz, M., and Pilling, M. J.: MESMER (Master Equation Solver for Multi-Energy Well Reactions), 2008–2012: An object oriented C++ program for carrying out ME calculations and eigenvalue-eigenvector analysis on arbitrary multiple well systems, available at: http://sourceforge.net/projects/mesmer (last access: 16 December 2016), 4.1 Edn., 2014.

Roscoe, H. K., Jones, A. E., Brough, N., Weller, R., Saiz-Lopez, A., Mahajan, A. S., Schoenhardt, A., Burrows, J. P., and Fleming, Z. L.: Particles and iodine compounds in coastal Antarctica, J. Geophys. Res.-Atmos., 120, 7144–7156, doi:10.1002/2015jd023301, 2015.

Saiz-Lopez, A. and Plane, J. M. C.: Novel iodine chemistry in the marine boundary layer, Geophys. Res. Lett., 31, L04112, doi:10.1029/2003GL019215, 2004.

Saiz-Lopez, A., Plane, J. M. C., Mahajan, A. S., Anderson, P. S., Bauguitte, S. J.-B., Jones, A. E., Roscoe, H. K., Salmon, R. A., Bloss, W. J., Lee, J. D., and Heard, D. E.: On the vertical distribution of boundary layer halogens over coastal Antarctica: implications for O_3, HO_x, NO_x and the Hg lifetime, Atmos. Chem. Phys., 8, 887–900, doi:10.5194/acp-8-887-2008, 2008.

Saiz-Lopez, A., Lamarque, J.-F., Kinnison, D. E., Tilmes, S., Ordóñez, C., Orlando, J. J., Conley, A. J., Plane, J. M. C., Mahajan, A. S., Sousa Santos, G., Atlas, E. L., Blake, D. R., Sander, S. P., Schauffler, S., Thompson, A. M., and Brasseur, G.: Estimating the climate significance of halogen-driven ozone loss in the tropical marine troposphere, Atmos. Chem. Phys., 12, 3939–3949, doi:10.5194/acp-12-3939-2012, 2012a.

Saiz-Lopez, A., Plane, J. M. C., Baker, A. R., Carpenter, L. J., Von Glasow, R., Gómez Martín, J. C., McFiggans, G., and Saunders, R. W.: Atmospheric Chemistry of Iodine, Chem. Rev., 112, 1773–1804, doi:10.1021/cr200029u, 2012b.

Saiz-Lopez, A., Fernandez, R. P., Ordóñez, C., Kinnison, D. E., Gómez Martín, J. C., Lamarque, J.-F., and Tilmes, S.: Iodine chemistry in the troposphere and its effect on ozone, Atmos. Chem. Phys., 14, 13119–13143, doi:10.5194/acp-14-13119-2014, 2014.

Saiz-Lopez, A., Baidar, S., Cuevas, C. A., Koenig, T. K., Fernandez, R. P., Dix, B., Kinnison, D. E., Lamarque, J. F., Rodriguez-Lloveras, X., Campos, T. L., and Volkamer, R.: Injection of iodine to the stratosphere, Geophys. Res. Lett., 42, 6852–6859, doi:10.1002/2015gl064796, 2015.

Sander, S. P., Friedl, R. R., Golden, D. M., Kurylo, M. J., Moortgat, G. K., Wine, P. H., Ravishankara, A. R., Kolb, C. E., Molina, M. J., Diego, S., Jolla, L., Huie, R. E., and Orkin, V. L.: Chemical Kinetics and Photochemical Data for Use in Atmospheric Studies Evaluation Number 15, JPL_NASA, 06-2, Jet Propulsion Laboratory, Pasadena, CA, 2006.

Sherwen, T., Evans, M. J., Carpenter, L. J., Andrews, S. J., Lidster, R. T., Dix, B., Koenig, T. K., Sinreich, R., Ortega, I., Volkamer, R., Saiz-Lopez, A., Prados-Roman, C., Mahajan, A. S., and Ordóñez, C.: Iodine's impact on tropospheric oxidants: a global model study in GEOS-Chem, Atmos. Chem. Phys., 16, 1161–1186, doi:10.5194/acp-16-1161-2016, 2016.

Simpson, W. R., Brown, S. S., Saiz-Lopez, A., Thornton, J. A., and Glasow, R. v.: Tropospheric Halogen Chemistry: Sources, Cycling, and Impacts, Chem. Rev., 115, 4035–4062, doi:10.1021/cr5006638, 2015.

Sommariva, R., Bloss, W. J., and von Glasow, R.: Uncertainties in gas-phase atmospheric iodine chemistry, Atmos. Environ., 57, 219–232, doi:10.1016/j.atmosenv.2012.04.032, 2012.

Šulková, K., Šulka, M., Louis, F., and Neogrády, P.: Atmospheric Reactivity of CH_2ICl with OH Radicals: High-Level OVOS CCSD(T) Calculations for the XAbstraction Pathways (X = H, Cl, or I), J. Phys. Chem. A, 117, 771–782, 2013.

Volkamer, R., Baidar, S., Campos, T. L., Coburn, S., DiGangi, J. P., Dix, B., Eloranta, E. W., Koenig, T. K., Morley, B., Ortega, I., Pierce, B. R., Reeves, M., Sinreich, R., Wang, S., Zondlo, M. A., and Romashkin, P. A.: Aircraft measurements of BrO, IO, glyoxal, NO_2, H_2O, O_2–O_2 and aerosol extinction profiles in the tropics: comparison with aircraft-/ship-based in situ and lidar measurements, Atmos. Meas. Tech., 8, 2121–2148, doi:10.5194/amt-8-2121-2015, 2015.

von Glasow, R., Sander, R., Bott, A., and Crutzen, P. J.: Modeling halogen chemistry in the marine boundary layer. 1. Cloud-free MBL, J. Geophys. Res., 107, 4341, doi:10.1029/2001JD000942, 2002.

Wachsmuth, M., Gäggeler, H. W., von Glasow, R., and Ammann, M.: Accommodation coefficient of HOBr on deliquescent sodium bromide aerosol particles, Atmos. Chem. Phys., 2, 121–131, doi:10.5194/acp-2-121-2002, 2002.

Wang, F., Saiz-Lopez, A., Mahajan, A. S., Gómez Martín, J. C., Armstrong, D., Lemes, M., Hay, T., and Prados-Roman, C.: Enhanced production of oxidised mercury over the tropical Pacific Ocean: a key missing oxidation pathway, Atmos. Chem. Phys., 14, 1323–1335, doi:10.5194/acp-14-1323-2014, 2014.